Torsional Strength Analysis of Universal Joint's ZP-11A due to Yokes Modification and Materials

Abstract

The study examined the strength of the universal joint after it was loaded with torsion. It used different materials that can withstand tensile stress in accordance with accepted principles and made modifications to the yoke as a result of the topology optimization process. The topology optimization determined that the yoke's part needed to withstand load without changing its dimensions and minimize stress distribution. According to the results, the maximum shear stress on the spider of the original universal joint model made of JIS-SF590A steel was 84.57 MPa, the shear stress on the yoke component was 30.84 MPa, and the maximum von Mises was 341.1 MPa. As a result of using JIS-SF590A steel, yoke modification 3 has produced a reduction in shear stress of 12.97% and a reduction in von Mises stress of 35.33% from the original yoke. This is the most efficient design of yoke and also this modified yoke form provides a wider elevation angle and is easier to manufacture.

Keywords: universal joint; topology optimization; shear stress; von Mises;.

I. Introduction

The azimuth thruster system, commonly known as the Z-Peller, is a propulsion system that is mounted vertically and has a 360⁰ degrees rotation. Their nozzle concentrates the water flowing around the blades. J. C. Kim et al. [1] looked into the maneuverability of the azimuth thruster system on the research vessel. Because of its capacity to rotate 360⁰, the Z-peller system has remarkably high maneuverability and efficiency. Some studies were carried out to study the material optimization of the steering yoke. The original universal joint and the modified universal joint with topology optimization were compared and evaluated in A. Koparde et al. [2] studied with the help of finite element software. The results showed that the modified yoke provided a uniform distribution across the entire structure. This resulted in a reduction of the maximum stress by 22.9% and a mass reduction of the yoke by 22.4% when compared to the original yoke. The failure might be brought on by unfavorable factors, including the environment, bad planning, or unstable torque loading. According to the study by NS Giridhar et al. [3], strong materials were selected and component dimensions were changed to reduce component stress and weight. The mechanism has the advantage of becoming simple to manufacture because it is constructed from two distinct sheet metals. Numerous mechanisms with various dimensions are created. Strong evidence suggests that the steel variant. The intricate

driving motion transmission consists of a long shaft with Cardan joints with variable geometry mounted on each end. The study by Chaban et al. provides a system of ordinary differential equations with a combined issue of Dirichlet first-type and Poincaré third-type boundary conditions is utilized to represent non-linear electromechanical differential equations [4].

The stress concentration can be reduced by fillet, but the amount of fillet provided should be optimum. Pastukhov et al. [5] using the WinShaft module in APM WinMachine, shaft design justification, and test computations are executed based on CAE tools. To decrease speed variations between the input and output shafts, the U-joints are arranged in a Z-configuration. The study by Bharti et al. is established that the Sommerfeld phenomenon, which is defined by resonance capture and escape by resonance, exists for significant parallel offsets between the input and output shafts. The escape by resonance is followed by a rapid increase in speed and a decrease in the amplitude of the torsional vibration. In reality, these jump phenomena happen at two separate speed ranges, one close to the inherent frequency of the U-joints' straight-line arrangement and the other at half of it. The rate at which the input shaft torque or power is changed has an impact on the dynamic response's nature, [6]. The universal joint components as

shown in Figure 1.

Zbigniew et al. [7] discovered that the elastic moment model might replicate true transient processes in the joint coordinates of the system by employing the fractional derivative integrator. Furthermore, it provides accuracy on par with the model with dispersed parameters. A modified Hamilton-Ostrogradski concept is implemented to create shaft equations, which are then utilized to analyze both the fully coupled system and the distributed parameter system. It is utilized to calculate rotational angles of shaft elements and essential analytical mechanics functions of the velocity continuum. Popenda et al. [8] investigated how the transmission shaft interacts between the working mechanism and the driving motor. The study by Ekemb et al. approachs relies on analogies among

bearing. Then, by using the modal synthesis method of substructures, the modal shapes of the shaft and the hull are integrated through the friction force to establish the nonlinear differential system of equations of the shaft-hull coupled system. After that, the self-excited vibration responses carried on by friction can be computed using the Runge-Kutta method to solve the nonlinear differential governing equations. On this base, the study by Wu et al. are held regarding how the friction coefficient, damping ratio, rotation speed, and support stiffness affect the shaft-hull coupled system's self-excited vibration. The results demonstrated that the difficulty of the shaft-hull coupled system's self-excited vibration would increase as damping, shaft speed of rotation, or supporting stiffness [11]. The poles encounter both shear and torsional force as a result of the forces that are
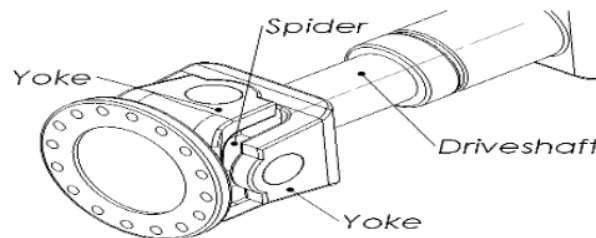

Figure 1. Universal joint components

mechanical and electrical systems. For the aforementioned transmission shaft, the equivalent circuits that are customary in electrical systems are defined. Long and flexible shafts, which are a regular feature of synchronous motors used in LCI technology, are extremely vulnerable to torsional vibration excite when their resonant frequency combine with any external load exerted on the shaft. International standards require a torsional analysis to assess the shaft's durability across the motor's entire speed range. Therefore, for such an evaluation, the motor air gap torque's frequency and magnitude are necessary [9].

The dynamic characteristics of a viscous-spring damper utilized to regulate the torsional vibration of the engine's shaft system, as well as the vibration characteristics of an ultra-long-stroke engine using de-rating technology, are reviewed in this study. Jaehoon et al. [10] recommended that the assigned probabilities for attempting to control torsional vibration in the propulsion shafting system would have to include adapting the design parameters of its dampening effect instead of using the optimum damper designed from concept to prevent fatigue fracture of shafts, in scenarios where ships have recently witnessed an engine acceleration issue in the critical zone. The Stribeck friction curve is applied to estimate the friction force between the shaft and the water-lubricated rubber

applied to them. Vehicles' motion transmission mechanisms are made up of a few sections, some of which occasionally encounter severe disappointments. A rotating part is generated when forces combine, and this section is vulnerable to fragility because of fluctuating torque. The two most important components of a car are the steering mechanism and the steering column. It is a critical element for achieving the vehicle's security and steady development. It has poles that have been shaped into a cross in the center of the roadway and had loads on each of its poles that were attached in the same manner as a cross joints. It experiences torsion force in adding to shear force as a result of forces placed on the cross-joint poles. Vehicles' movement transmission systems are formed of a few parts, some of which can suffer severe disappointments [12].

According to the study of Cardoso et al. [13], the manufacturing process and material design, specifically the amount, location, and roughness of mechanical stakes and forks, as well as the content of microstructure inclusions, are variables that could affect fatigue life in this automobile component. A computer-aided multibody modeling approach for the simulation of a Cardan joint with manufacturing errors was studied by Cirelli et al. [14]. During the modeling phase, the elasticity of flexible bodies is lumped and the joint compliance is taken into account using concentrated non-linear spring elements.

The torsional fluctuations in the flexible coupling dramatically increased and then abruptly ceased. The coupling connected to the intermediate shaft did not have sufficient radial flexibility to dampen these vibration. The study of Song et al. [15] concluded that to avoid the effects of the self-excited torsional vibration, it is recommended that this coupling is replaced with one that is capable of absorbing the radial shaft displacement. Investigation of a parallel manipulator with Cardan and prismatic joints was studied by Augi et al. [16]. It is recommended that the layout involves a relatively stiff and robust structure. The manipulator is supposed to be moved by direct-drive linear actuators. This choice is justified by the possibility of accurate control of heavy insertion losses. This is done by simplifying or removing a large part of the additional actuation and sensing systems that are normally installed on conventional machines. According to the residual threshold of the associated linear systems, both reduced-order bases are enriched, and the grid resolution is adaptively determined based on the relative inaccuracy in approximating the objective function and constraint values throughout the iteration. With acceptable goal and constraint violation errors, the tests on benchmark 2D and 3D show increased performance. The impact of important stress constraint factors, thus the allowable stress value, stress penalty factor, and p-norm factor, is carefully examined by Xiao et al. [17]. The gradients necessary to carry out the optimization could be computed relatively fast using the adjoint approach. Gregor et al. [18] have successfully derived the gradients using a "first optimize then discretize" scheme. By enhancing the topology both of hard and soft magnetic thin film structures, the method's capabilities are proven, and the outcomes are confirmed by comparison with an analytical solution.

References from previous studies and cases of mechanical failures involving universal joints are provided. Using ship shaft data, one may perform a static analysis of a universal joint to calculate the shear stress, von Mises, and safety factor. The yoke should be optimized by static simulations with a variety of materials that fulfill the tensile strength requirement rule. Due to modifications in the form of the yoke and the material used to construct it, we will analyze the torsion strength of the universal joint.

II. Materials and Methods

A. Data

To examine this study, the universal joint assembly model should be created. Before doing an analysis, the dimensions of the universal joint components should be determined. The dimensions of the universal joint assembly used in this study are shown in Table 1.

Table 1.
Dimension of Universal Joint Assembly

Part	Dimension
Shaft Diameter	130 mm
Universal Joint Length	1100 mm
Universal Joint Diameter	260 mm
Elevation Angle	5.73^0
Bolt Type	M20 x 2.5 x 80
Flange Length	381.5 mm
Flange Outside Diameter	350 mm

B. Material variations

JIS-SF590A was chosen as a material for the original yoke. Based on the BKI rule, we will use other materials for variation of materials in this study, where materials for shafting components must have a tensile strength of 400-800 MPa, as shown in Table 2.

Table 2.
Material's mechanical properties

Mechanical Properties	ASTM A36	JIS-SF590A	AISI Stainless Steel 316L	SS41 (Bolt-Nut)
Tensile strength	400 MPa	590 MPa	485 MPa	475 MPa
Yield strength	250 MPa	295 MPa	170 MPa	225 MPa
Density	7,850 kg.m^{-3}	7,800 kg.m^{-3}	8,000 kg.m^{-3}	7,800 kg.m^{-3}
Poisson Ratio	0.26	0.29	0.3	0.3
Elastic Modulus	200 GPa	200 GPa	173 GPa	210 GPa

C. Yoke variations

The yoke component makes an elevation angle at installation possibly. The modification of the yoke shape is considered to result in a reduced yoke mass, make manufacturing easier, and increase the elevation angle of installation. The yoke variations that will be applied involve modifying the original ship yoke shape. This will involve several modified yoke forms based on the topology optimization results and another yoke form from the previous study. The yoke variations are shown in Figure 2.
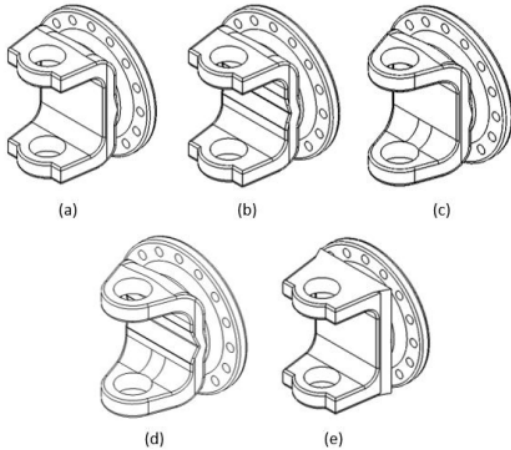
Figure 2(a) original yoke, (b) yoke modification 1, (c) yoke modification 2, (d) yoke modification 3, (e) yoke modification 4

The design of Figure 2(a) shows the default yoke installed on the tug boat, for the shape of the yoke in design modification 3 in Figure 2(d) looks at the results of the topology study that has been done. The modified model 4 in Figure 2(e) is based on the yoke shape in the research conducted by Y. Richard et al. [5]. Meanwhile, the cutting of the middle cross-section of the yoke with dimensions of 80 mm x 10 mm in Figure 2(b) and Figure 2(d) sees the distribution of low stress from the simulation results.

D. Boundary condition and loading condition

Using SOLIDWORKS 2020, 3D finite element model was generated. The shape of the solid meshed with tetrahedral cell technology. Tetrahedral cells are very effective for solid structures because they are flexible and adapt to irregular or curved shapes. The application will support multi-core surface and volume meshing using curvature base mesh. It is excellent for meshing complex structures. Figure 3 shows the mesh on the model.
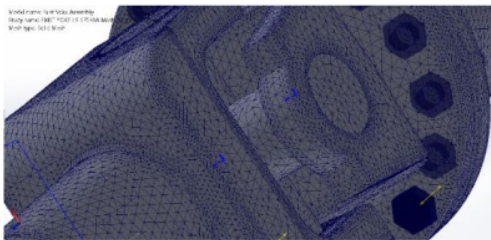

Figure 3. Meshing of model

The torque of the main engine is calculated by dividing the power and rpm of the main engine [19]. At the flange connected to the main engine, the torque of 15,174.96 Nm was given at the flange connected to the main engine as shown in Figure 4. In addition, boundary conditions were applied at the flange connected to the intermediate shaft, as shown in Figure 5.
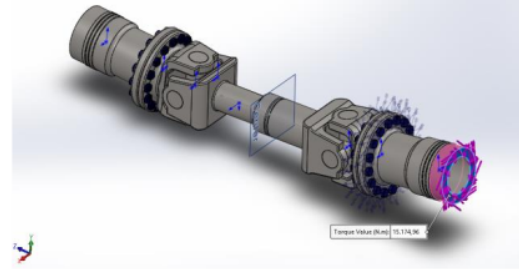

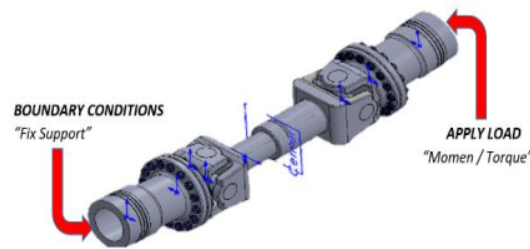Figure 4. Apply moment torque location

Figure 5. Boundary condition and moment location

At the flange attached to the intermediate shaft, all motions were fixed. Static structural analysis was carried out using SOLIDWORKS 2020 solver.

E. Mesh convergence

Mesh convergence is a method for comparing the most stable results for each element size from several stress analysis results with various element sizes. The convergence is carried out to evaluate the software's precision. Figure 6 shows the convergence of the mesh elements.
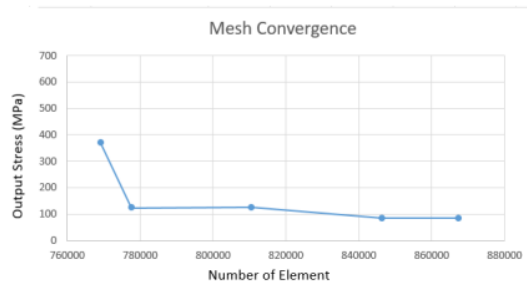

Figure 6. Graph of mesh convergence

At meshing diameters between 10 mm and 9 mm, mesh convergence is obtained. A meshing size of 10 m is determined with a stress value of

84.55 MPa based on the convergence results.

III. Results and Discussion

A. Topology optimization of the original yoke

The optimization of the yoke is discovered using the topology optimization method. This method offers the most efficient material layout for design and loading. The SOLIDWORKS 2020 Topology Optimization Study was used to observe the element density distribution for the original yoke and identify the low-stress regions shown in Figure 7.
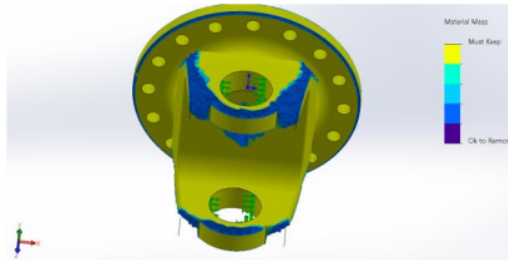

Figure 7. Yoke Topology Study

The low-stress areas that can be eliminated by paying attention to manufacturing lines, as well as certain functional constraints are shown in Figure 7. The dead zone, as seen in the blue area, is where components from that region do not contribute to the workload and, therefore, can be eliminated. It must remain in the yellow area because it is required to withstand the workload placed on the models.

B. Simulation result on the original yoke of universal joint

The torque of the main engine is calculated by dividing the power and rpm of the main engine [19]. At the flange connected to the main engine, the torque of 15,174.96 Nm was given and the component was analyzed for the strength of the models. From the simulation results using the software, the largest values of shear stress and von Mises stress are obtained. In the ship's universal joint assembly model using JIS-SF590A material, the maximum shear stress is 84.57 Mpa, located on the spider shown in Figure 8. The shear stress on the yoke is 30.84 MPa and the maximum von Mises stress is 341.1 MPa located on the yoke, as shown in Figure 9.
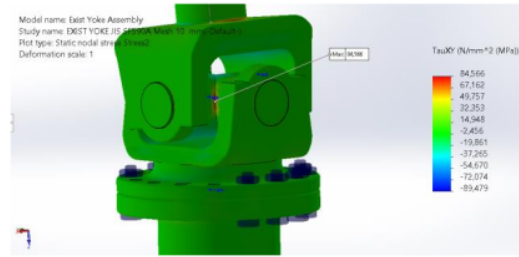

Figure 8. The simulation analysis results of shear stress on the original universal joint
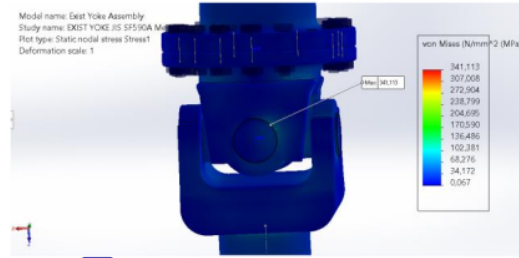

Figure 9. The simulation analysis results of von Mises on the original universal joint

C. Simulation result on the yoke modifications

1. Comparison of shear stress result

The modified yoke was analyzed for the same boundary conditions, and shear stress and von Mises stress results were observed. The shear stress and von Mises distribution of the modified yoke are shown in Figures 10 and 11, respectively.
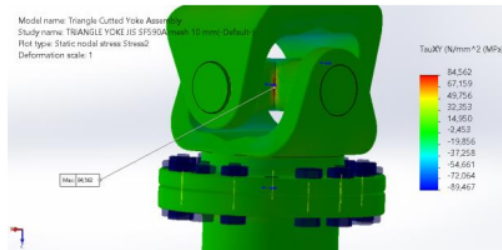

Figure 10. The simulation analysis results of shear stress on the modified yoke

The critical point in each model variation lies in the spider component. The shear stress results from static simulation for each model variation are presented in Tables 3-5.

Table 3.
Comparison of shear stress of each model with ASTM A36 steel

Model	Yoke (MPa)	Spider (MPa)	Driveshaft (MPa)	Flange (MPa)
Original Yoke Model	29.1	85.64	42.42	20.17
Yoke Modification 1	28.44	84.96	86.75	20.28
Yoke	27.32	84.84	41.69	20.15

Model	Yoke (MPa)	Spider (MPa)	Driveshaft (MPa)	Flange (MPa)
Modification 2 Yoke	27.13	84.89	38.54	20.28
Modification 3 Yoke	27.92	84.79	85.35	20.15
Modification 4				

The maximum shear stress obtained using the model's variation is significantly below the ASTM A36 material's yield strength 250 MPa. The reduction of shear stress on the yoke is 6.77% compared with the original yoke, as shown in the modified model of yoke 3.

Table 4.
Comparison of shear stress of each model with JIS-SF590A steel

Model	Yoke (MPa)	Spider (MPa)	Driveshaft (MPa)	Flange (MPa)
Original Yoke Model	30.84	84.57	43.33	21.05
Yoke Modification 1	28.08	84.63	85.85	21.3
Yoke Modification 2	27.03	84.52	41.36	21.04
Yoke Modification 3	26.84	84.56	38.45	21.29
Yoke Modification 4	27.63	84.47	84.54	21.04

The maximum stress obtained in the model variation is significantly lower than the 295 MPa yield strength of the JIS-SF590A material. The shear stress on the yoke of the modified model 3 has been reduced by 12.97%.

Table 5.
Comparison of shear stress of each model with AISI Stainless Steel 316L

Model	Yoke (MPa)	Spider (MPa)	Driveshaft (MPa)	Flange (MPa)
Original Yoke Model	29.37	84.84	42.41	20.31
Yoke Modification 1	28.38	84.91	86.6	20.45
Yoke Modification 2	27.27	84.79	41.68	20.3
Yoke Modification 3	27.01	84.84	38.53	20.3
Yoke Modification 4	27.87	84.74	85.22	20.3

The maximum stress obtained in the model variation is significantly lower than 170 MPa yield strength for AISI Stainless Steel 316L material. The shear stress reduction on the yoke is 8.035%, which can be seen in the modified model of yoke 3. The results obtained by numerical analysis of the stress distribution at the input yoke of the universal joint showed that even small variations in shape could cause significant variations in the stress distribution. Therefore, topology optimization is carried out to obtain the efficiency of stress distribution on the yoke. The case with the lowest voltage level is identified and selected as the most profitable design solution. Based on the shear stress analysis results from all the variations presented, the yoke modification 3 with JIS-SF590A steel has the greatest stress reduction compared to other variations, amounting to 12.97%.
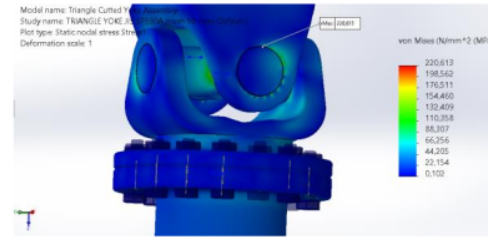
2. Comparison of Von Mises Result

Figure 11. The simulation analysis results of von mises on the modified yoke

The critical point of von Mises stress in each variation model lies in the eye pad of the yoke component. The results of von Mises stress simulation results for each model variation are presented in Tables 6- 8.

Table 6.
Comparison of von Mises stress of each model with ASTM A36 steel

Model	Yoke (MPa)	Spider (MPa)	Driveshaft (MPa)	Flange (MPa)
Original Yoke Model	348.8	184.8	173.1	53.81
Yoke Modification 1	229.3	184.9	157.3	53.9
Yoke Modification 2	351.1	184.7	150.3	54.8
Yoke Modification 3	227.4	184.7	155.9	53.89
Yoke Modification 4	277.1	184.2	149.8	53.81

The von Mises stress has been reduced by 34.81% using the modified model of yoke 3 compared to the ship's original yoke.

Table 7.
Comparison of von Mises stress of each model with JIS-SF590A steel

Model	Yoke (MPa)	Spider (MPa)	Driveshaft (MPa)	Flange (MPa)
Original Yoke Model	341.1	181.9	172.1	53.5
Yoke Modification 1	222.9	182	156.2	53.57
Yoke Modification 2	338.5	181.8	150	53.49
Yoke Modification 3	220.6	181.8	155.5	53.56
Yoke Modification 4	270.5	181.8	149.9	53.5

It can be seen that when compared to the ship's original yoke, the modified yoke 3 model

has 35.33% von Mises stress reduction.

Table 8.
Comparison of von Mises stress of each model with AISI Stainless Steel 316L

Model	Yoke (MPa)	Spider (MPa)	Driveshaft (MPa)	Flange (MPa)
Original Yoke Model	344.2	184.3	172.9	53.76
Yoke Modification 1	228.3	184.4	157.3	53.85
Yoke Modification 2	249.2	184.2	150.2	53.75
Yoke Modification 3	226.5	184.2	124.5	53.83
Yoke Modification 4	276.2	184.2	149.9	53.75

Compared to the ship's original yoke, the redesigned model of yoke 3 has a 34.20% lower von Mises stress. The results of the numerical analysis of the stress distribution at the universal joint's input yoke revealed that even minor shape changes may result in significant modifications in the stress distribution. The yoke modification 3 with JIS-SF590A steel has the greatest stress reduction compared to other variations, equal to 35.33%, based on the von Mises stress analysis results from all the variants shown.

3. Comparison of safety factors

The safety factor criteria for universal joint components based on the BKI rule that applies to main shafting components is 1 [20]. The safety factor calculation can be obtained compared to the yield strength of the material with the results of von Mises stress must be higher than 1 [19]. Components like the yoke, spider, and driveshaft of universal joints must comply with that safety factor criteria. Figure 12 shows the yoke safety factor data for each model. It is known that only modifications 1, 3, and 4 ,manufactured with JIS-SF590A material, as well as modifications model 3 manufactured of ASTM A36, are yoke components that fulfill the safety factor criteria. Figure 13 shows the spider safety factor. Only the original yoke model and the variations of yoke modification with AISI Stainless Steel 316L are the spider components that do not fulfill the safety factor criteria. Figure 14 shows the driveshaft safety factor. According to the BKI rule, which applies to main shafting components, the safety factor requirement for universal joint components is 5 [20]. It can be seen that the flange components comply with the safety factor criteria for all models. Figure 15 shows the results of the safety factor of the flange for each model.
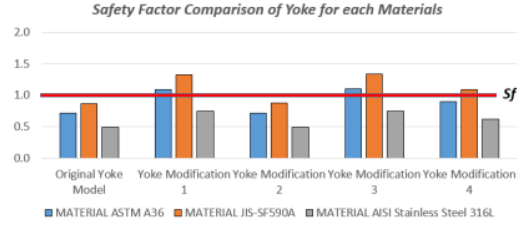

Figure 12.
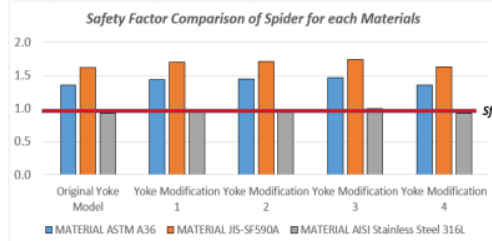Graph of yoke component safety factor with several materials.

Figure 13.
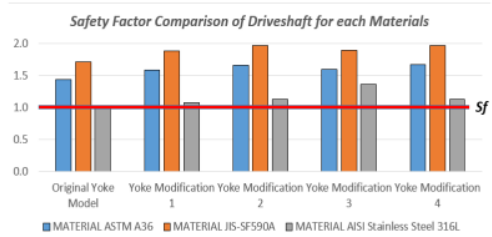Graph of spider component safety factor with several materials.

Figure 14.
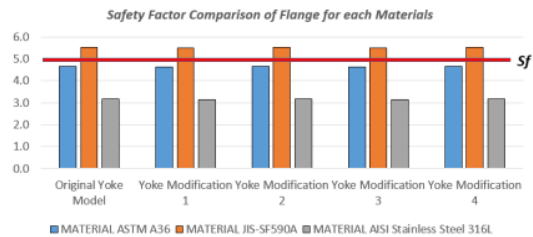Graph of driveshaft component safety factor with several materials.

Figure 15.
Graph of flange component safety factor with several materials.

IV. Conclusions

Based on the analysis results, it can be concluded that the JIS-SF590A material used in the ship's universal joint model has maximum shear stress of 30.84 MPa and a von Mises stress of 341.1 MPa, which is found on the eye yoke pad. The original yoke will

obtain the element density of stress distribution by topology optimization. In the modified yoke 3 models, there is a reduction of 35.33% in von Mises and 12.97% in the shear stress of the yoke component, respectively. Each universal joint component made of ASTM A36 and JIS-SF590A materials has fulfilled the safety factor criteria. The modified yoke 3 has a very good shape in terms of strength because it has minimal stress. Its design also provides a greater elevation angle than the original ship yoke model, making it easier to manufacture and install.

References

[1] J.-C. KIM, I.-K. KANG, J.-H. LEE, S.-J. HAM, C.-W. PARK, and S.-H. KIM, "The maneuvering characteristics of the research vessel NARA equipped with the azimuth thruster system," *J. Korean Soc. Fish. Technol.*, vol. 53, no. 3, pp. 276–285, 2017, doi: 10.3796/ksft.2017.53.3.276.

[2] A. Koparde, N. Mithra, and S. Ahankari, "Numerical and experimental analysis of torsional stress of traditional and modified steering yoke," *Mater. Today Proc.*, vol. 46, pp. 7099–7104, 2021, doi: 10.1016/j.matpr.2020.10.167.

[3] N. S. Giridhar, S. Hetawal, and P. Baskar, "Finite Element Analysis of Universal Joint and Propeller Shaft Assembly," vol. 5, no. 5, pp. 226–229, 2013.

[4] A. Chaban, Z. Łukasik, A. Popenda, and A. Szafraniec, "Mathematical modelling of transient processes in an asynchronous drive with a long shaft including cardan joints," *Energies*, vol. 14, no. 18, 2021, doi: 10.3390/en14185692.

[5] A. Lozynskyy, A. Chaban, T. Perzyński, A. Szafraniec, and L. Kasha, "Application of fractional-order calculus to improve the mathematical model of a two-mass system with a long shaft," *Energies*, vol. 14, no. 7, 2021, doi: 10.3390/en14071854.

[6] S. K. Bharti and A. K. Samantaray, "Resonant capture and Sommerfeld effect due to torsional vibrations in a double Cardan joint driveline," *Commun. Nonlinear Sci. Numer. Simul.*, vol. 97, p. 105728, 2021, doi: 10.1016/j.cnsns.2021.105728.

[7] Ł. Zbigniew, C. Andriy, S. Andrzej, and Ż. Vołodymyr, "Model matematyczny układu napędowego z silnikiem asynchronicznym i pompą pionową," *Prz. Elektrotechniczny*, vol. 94, no. 1, pp. 133–138, 2018, doi: 10.15199/48.2018.01.34.

[8] A. Popenda, M. Lis, M. Nowak, and K. Blecharz, "Mathematical modelling of drive system with an elastic coupling based on formal analogy between the transmission shaft and the electric transmission line," *Energies*, vol. 13, no. 5, 2020, doi: 10.3390/en13051181.

[9] G. Ekemb, F. Slaoui-hasnaoui, J. Song-manguelle, P. M. Lingom, and I. Fofana, "Instantaneous electromagnetic torque components in synchronous motors fed by load-commutated inverters," *Energies*, vol. 14, no. 11, 2021, doi: 10.3390/en14113223.

[10] J. Jee, C. Kim, and Y. Kim, "Design improvement of a viscous-spring damper for controlling torsional vibration in a propulsion shafting system with an engine acceleration problem," *J. Mar. Sci. Eng.*, vol. 8, no. 6, 2020, doi: 10.3390/JMSE8060428.

[11] C. Wu, F. Chen, and X. Long, "The self-excited vibration induced by friction of the shaft-hull coupled system with the water-lubricated rubber bearing and its stick-slip phenomenon," *Ocean Eng.*, vol. 198, p. 107002, 2020, doi: 10.1016/j.oceaneng.2020.107002.

[12] A. Kohli, M. Hombalmath, A. Y. Patil, and P. C. Aruna Kumara, "Analysis of universal joint using virtual simulation method," *Mater. Today Proc.*, vol. 59, pp. 858–866, 2022, doi: 10.1016/j.matpr.2022.01.213.

[13] A. S. M. Cardoso *et al.*, "Fatigue resistance performance of universal cardan joint for automotive application," *Eng. Fail. Anal.*, vol. 135, no. February, p. 106128, 2022, doi: 10.1016/j.engfailanal.2022.106128.

[14] M. Cirelli, V. Rossi, P. P. Valentini, and E. Pennestrì, "A dynamic model of a Cardan joint to evaluate the effect of elasticity and manufacturing errors," *Int. J. Veh. Perform.*, vol. 7, no. 1–2, pp. 136–155, 2021, doi: 10.1504/IJVP.2021.113423.

[15] M. Song, T. Nam, and J. Lee, "Self-Excited Torsional Vibration in the Flexible Coupling of a Marine Propulsion Shafting System Employing Cardan Shafts," pp. 1–13, 2020, doi: 10.3390/jmse8050348.

[16] L. Pugi, L. Fiorineschi, and F. Rotini, "Preliminary design investigation of a rrprr parallel manipulator with cardan joint and direct drive actuation," *IEEE/ASME Int. Conf. Adv. Intell. Mechatronics, AIM*, vol. 2021-July, pp. 1207–1212, 2021, doi: 10.1109/AIM46487.2021.9517628.

[17] M. Xiao, J. Ma, D. Lu, B. Raghavan, and W. Zhang, "Stress-constrained topology optimization using approximate reanalysis with on-the-fly reduced order modeling," *Adv. Model. Simul. Eng. Sci.*, vol. 9, no. 1, 2022, doi: 10.1186/s40323-022-00231-x.

[18] G. Wautischer, C. Abert, F. Bruckner, F. Slanovc, and D. Suess, "A topology optimization algorithm for magnetic structures based on a hybrid FEM–BEM method utilizing the adjoint approach," *Sci. Rep.*, vol. 12, no. 1, pp. 1–11, 2022, doi: 10.1038/s41598-021-04246-z.

[19] E. P. Popov, "Mechanics of Solids," p. 106, Prentice Hall Inc., 2nd edition, 1976. [Online]. Available: http://www.vssut.ac.in/lecture_notes/lecture1423904647.pdf

[20] BKI, "RULES FOR MACHINERY INSTALLATIONS Edition 2021," vol. VI, 2021. [Online]. Available: https://servrules.bki.co.id:81/data/(%20Vol%20III%20),2022%20Rules%20for%20Machinery%20Installations%20(EN),2022.pdf

5921.docx

ORIGINALITY REPORT

17%
SIMILARITY INDEX

PRIMARY SOURCES

1. Anand Koparde, Nithin Mithra, Sandeep Ahankari. "Numerical and experimental analysis of torsional stress of traditional and modified steering yoke", Materials Today: Proceedings, 2020
   Crossref — 110 words — 3%

2. www.researchgate.net
   Internet — 108 words — 3%

3. trid.trb.org
   Internet — 90 words — 2%

4. ras.papercept.net
   Internet — 60 words — 1%

5. www.mdpi.com
   Internet — 59 words — 1%

6. Saurabh K. Bharti, A.K. Samantaray. "Resonant Capture and Sommerfeld Effect Due to Torsional Vibrations in a Double Cardan Joint Driveline", Communications in Nonlinear Science and Numerical Simulation, 2021
   Crossref — 54 words — 1%

7. Hadiseh Karimaei, Hamidreza Chamani. "Parametric Study of Torsional Damper on Crankshaft Life Assessment of an IC Engine", International Journal of Reliability, Risk and Safety: Theory and Application, 2020
   Crossref — 29 words — 1%

8   amses-journal.springeropen.com
     Internet   29 words — 1%

9   S.-T. Wang, R. Wahrer, F. Anet, C.J. Chen et al. "A
     preliminary design for a one GHz NMR   20 words — < 1%
     spectrometer magnet", IEEE Transactions on Magnetics, 1994
     Crossref

10   constellation.uqac.ca
     Internet   16 words — < 1%

11   Gregor Wautischer, Claas Abert, Florian Bruckner,
     Florian Slanovc, Dieter Suess. "A topology   14 words — < 1%
     optimization algorithm for magnetic structures based on a
     hybrid FEM–BEM method utilizing the adjoint approach",
     Scientific Reports, 2022
     Crossref

12   autodocbox.com
     Internet   14 words — < 1%

13   Junchao Zhu, Guangcheng Wei, Zilong Peng,
     Zhaowang Xia, Liangyan Zheng, Hanhua Zhu.   13 words — < 1%
     "Analysis of underwater explosion shock on ship shaft stern
     bearing lubrication characteristics under different bearing
     working conditions", International Journal of Naval Architecture
     and Ocean Engineering, 2022
     Crossref

14   Manyu Xiao, Jun Ma, Dongcheng Lu, Balaji
     Raghavan, Weihong Zhang. "Stress-Constrained   12 words — < 1%
     Topology Optimization Using Approximate Reanalysis with on-
     the-Fly Reduced Order Modeling", Research Square Platform
     LLC, 2021
     Crossref Posted Content

15   Cui, Yan, Yu Liu, and N Zhao. "Research on application of green building technologies in designs of school", Advances in Civil Engineering and Building Materials, 2012.
Crossref

     9 words — < 1%

16   Feng Guo, Junwu Wang, Denghui Liu, Yinghui Song. "Evolutionary Process of Promoting Construction Safety Education to Avoid Construction Safety Accidents in China", International Journal of Environmental Research and Public Health, 2021
Crossref

     9 words — < 1%

17   svf2.uniza.sk
Internet

     9 words — < 1%

18   Amir Syawal Kamis, Ahmad Faizal Ahmad Fuad, Azmirul Ashaari, Che Wan Mohd Noor, Sheikh Alif Ali. "Development of WOP Mathematical Model for Optimum Track-Keeping. A Ship Simulation Study Using VLCC, Focusing on Hard Over Rudder Turning Circle with Three Stages of Validation Analysis", Polish Maritime Research, 2021
Crossref

     8 words — < 1%

19   C. Shyamlal, S. Rajesh. "Friction stir welding: A mathematical review", AIP Publishing, 2022
Crossref

     8 words — < 1%

20   Erwin V. Zaretsky, Harold H. Coe, Richard August. "Effect of Hoop Stress on Ball Bearing Life Prediction©", Tribology Transactions, 1997
Crossref

     8 words — < 1%

21   Yue-Peng Zhang, Guang-Zhong Cao, Zi-Qin Ling, Bin-Bin He, Hao-Ran Cheng, Wen-Zhou Li, Sheng-Bin Cao. "A Real-Time Gait Phase Recognition Method Based on

     8 words — < 1%

Multi-Information Fusion", 2021 18th International Conference on Ubiquitous Robots (UR), 2021
Crossref

22   ethesis.nitrkl.ac.in
     Internet   8 words — < 1%

23   Lifang Qiu, Gang Huang, Siqi Yin. "Design and
     Performance Analysis of Double C-Type Flexure   7 words — < 1%
     Hinges", Journal of Mechanisms and Robotics, 2017
     Crossref

EXCLUDE QUOTES   OFF   EXCLUDE SOURCES   OFF
EXCLUDE BIBLIOGRAPHY   ON   EXCLUDE MATCHES   OFF